Science of the Total Environment 826 (2022) 153922

Contents lists available at ScienceDirect

Science of the Total Environment

journal homepage: www.elsevier.com/locate/scitotenv

Symbiont-induced intraspecific phenotypic variation enhances plastic trapping and ingestion in biogenic habitats

Katy R. Nicastro [a,b,c], Laurent Seuront [a,c,d], Christopher D. McQuaid [c], Gerardo I. Zardi [c,*]

[a] Univ. Lille, CNRS, Univ. Littoral Côte d'Opale, UMR 8187 – LOG – Laboratoire d'Océanologie et de Géosciences, F-59000 Lille, France
[b] CCMAR–Centro de Ciencias do Mar, CIMAR Laboratório Associado, Universidade do Algarve, Campus de Gambelas, Faro 8005-139, Portugal
[c] Department of Zoology and Entomology, Rhodes University, Grahamstown 6140, South Africa
[d] Department of Marine Resources and Energy, Tokyo University of Marine Science and Technology, 4-5-7 Konan, Minato-ku, Tokyo 108-8477, Japan

HIGHLIGHTS

- Intraspecific variation is one of the most fundamental components of biodiversity.
- It is largely unknown whether plastic pollution affects intraspecific variation.
- We focused on symbiont-induced phenotypic variation in reef building mussel species.
- Symbionts significantly increase reef complexity, microplastic trapping and ingestion.
- Intraspecific variation shapes plastic pollution at the ecosystem level.

GRAPHICAL ABSTRACT

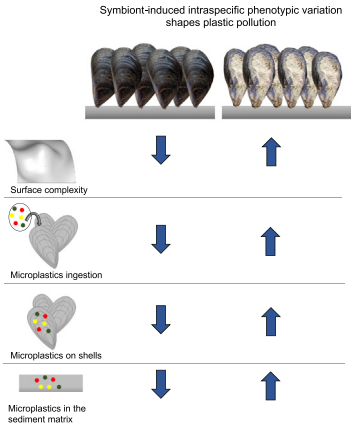

ARTICLE INFO

Article history:
Received 10 November 2021
Received in revised form 25 January 2022
Accepted 12 February 2022
Available online 17 February 2022

Editor: Dimitra A Lambropoulou

Keywords:
Mussel
Mytilus
Endoliths
Intertidal
Parasite
Plastic pollution

ABSTRACT

Plastic contamination has major effects on biodiversity, enhancing the consequences of other forms of global anthropogenic disturbance such as climate change and habitat fragmentation. Despite this and the recognised importance of intraspecific diversity, we still know relatively little about how plastic pollution affects diversity below the species level. Here, we assessed the effects of intraspecific variation in a habitat forming species (the Mediterranean mussel *Mytilus galloprovincialis*) on the trapping and ingestion of microplastics. We focused on symbiont-induced phenotypic variation in mussel beds. Using fractal analysis, we measured an increase in the complexity of mussel bed surfaces by ca. 15% caused by phototropic shell-degrading endoliths. By simulating high tide flow conditions and incoming waves, we found that symbionts significantly increased microplastic accumulation in mussel beds. This likely reflects deceleration of near-bed flow velocities, creation of turbulence in the bottom boundary layer and consequently increased particle retention. This effect was not constant at high tide, with no effect of infestation on retention at the base of the mussel bed under mid and high flow conditions and reduced microplastic trapping on the surface of mussel shells. Nevertheless, under natural conditions, the ingestion and trapping of microplastic were higher by the mussels comprising beds with symbionts than those in beds without symbionts. Given the dependency of many species on mussel biogenic habitats, there is an increased risk of plastics moving up the food chain in mussel beds infested by symbiotic endoliths. Our results highlight how the effects of within-species phenotypic diversity may influence the consequences of rising levels of plastic pollution.

* Corresponding author.
E-mail address: zardi73@yahoo.it (G.I. Zardi).

http://dx.doi.org/10.1016/j.scitotenv.2022.153922

1. Introduction

Intraspecific variation is one of the most fundamental components of biodiversity, yet early research assessing the impacts of human-induced climate change on biodiversity largely overlooked variation below the species level. Only recently has mounting theoretical and empirical evidence shown that most often species do not respond as single, homogenous units to climate change-related threats and that variation below the species level plays a fundamental role in ecological and evolutionary processes, including responses to environmental change (Saada et al., 2016; Hurtado et al., 2020) the maintenance of overall diversity (Lourenço et al., 2016; Lourenço et al., 2017a; Ntuli et al., 2020), and ecological stability and resilience (Des Roches et al., 2018; Nicastro et al., 2020).

Plastic contamination is rapidly emerging as a worldwide threat. Since mass production of plastic took off in modern society, the inadequate management of its waste has increasingly jeopardised biodiversity. Interspecific differences in response to plastic pollution have been highlighted in numerous studies (e.g., Green et al., 2016; Law, 2017; Seuront et al., 2020), but, as with early research on the effect of climate changes, studies on plastic litter have, so far, mostly assumed that species are ecologically and physiologically homogenous units. Such generalisation ignores variation below the species level, potentially underestimating and oversimplifying the effects of plastics in the environment. Failure to detect population-level or within-population level effects may mask subtle, but important, within-species responses that may be crucial for the assessment of the impact of plastic pollution at the species level.

Marine biogenic habitats are three-dimensional structures created by the presence of species that form new complex habitats such as coral reefs, seagrass and mussel beds, or mangrove and kelp forests. The structural and functional characteristics of such species provide vital ecosystem functions and services that support human well-being. For instance, they support biodiversity, provide “blue carbon” storage by acting as carbon sinks (e.g., Krause-Jensen et al., 2018), contribute to nutrient and biogeochemical cycling (e.g., Lacoste et al., 2019), and promote secondary and tertiary production (Lim et al., 2020). Furthermore, biogenic habitats are a direct source of food and biotic raw materials, used as fertilizer and wood, and offer protection against coastal erosion and waves (Loh et al., 2019). Yet, all of these biogenic habitats are under serious threat. On one hand, they experience particularly strong non-climatic anthropogenic pressure from dense human populations, which are concentrated in coastal areas (e.g., Gillson et al., 2013; Kaplan-Hallam et al., 2017; Nicastro et al., 2018). At the same time, they are particularly vulnerable to long-term warming (e.g., Nicastro et al., 2013; Mota et al., 2015) and extreme climatic events such as heat waves (e.g., Seuront et al., 2019; Smale et al., 2019). There is now also overwhelming evidence that plastic contamination has major effects on biogenic habitats, contributing to the stress of other forms of global anthropogenic disturbance, such as rising temperatures, ocean acidification and habitat fragmentation (Green et al., 2016; Huang et al., 2020; Seuront et al., 2020). Because numerous species and ecological processes depend on biogenic habitats, accumulation of plastic litter in the ecosystems they sustain can have several significant consequences. These include transfer of ingested microplastic to higher trophic levels (Farrell and Nelson, 2013; Khan and Prezant, 2018), biomagnification of leaching contaminants (Mato et al., 2001; Teuten et al., 2009), and increased vulnerability to biotic and abiotic stressors such as predators and waves (Green et al., 2016; Green et al., 2019; Seuront et al., 2020). Additionally, microplastic ingestion can influence the ecological functioning of biogenic habitats by reducing the diversity and abundance of the associated fauna (e.g., Green et al., 2016).

In this context, structural features of biogenic habitats play a crucial role. Features such as surface roughness and spatial arrangement can significantly alter hydrodynamics over a surface by decreasing water flow speed and generating turbulent mixing (Butman et al., 1994; Green et al., 1998). Such effects can significantly influence the retention and accumulation of particles, ultimately affecting sedimentation, larval recruitment and food uptake by filter-feeders (Widdows et al., 1998; Lapointe and Bourget, 1999; Fuchs and Reidenbach, 2013). Recent evidence shows that such changes in water flow and turbulence also increase the vulnerability of biogenic habitats to microplastic trapping and ingestion (e.g., Khan and Prezant, 2018; Nel and Froneman, 2018; Cozzolino et al., 2020). For instance, in cold-water corals, the degree of microplastic trapping is enhanced by the species-specific complexity of the three-dimensional structure of coral colonies (D’Onghia et al., 2017). Similarly, macro- and microplastic trapping in multiple coastal vegetated habitats is influenced by interspecific differences in canopy properties, such as shoot height, density or stiffness (Cozzolino et al., 2020). Despite these marked species-specific effects, to our knowledge, no study has assessed the effect of different phenotypic structural variability within a species on plastic trapping.

In this study, we focus on the effect of symbiont-induced intraspecific phenotypic variation in an intertidal mussel biogenic habitat. Within-species phenotypic variation can be produced by genetic differences, stochastic developmental events and by abiotic and biotic components of the environment. Numerous experimental and observational studies have shown that, among the biotic components, symbiotic interactions, both parasitic and mutualistic, can alter the host's experience of environmental stress by altering the host phenotype (Feldhaar, 2011). This is the case for the widespread symbiosis between shell-degrading endoliths and intertidal mussels. In intertidal mussel beds, phototrophic shell-degrading endoliths (mainly cyanobacteria) significantly corrode mussel shells and modify the structure and microhabitat conditions within mussel assemblages (Lourenço et al., 2017b). With increasing endolithic activity, grooves and pits appear on the shell surface and eventually, at the highest levels of infestation, the shell becomes heavily pitted, deformed and eventually collapses, usually in the area above the adductor muscle (Kaehler and McQuaid, 1999).

Here, we ask whether endolith-induced phenotypic variation of shell microtopography in an important biogenic reef forming species, the Mediterranean mussel *Mytilus galloprovincialis*, affects microplastic accumulation within the mussel bed structure and microplastic presence in the mussels comprising the bed. Using a series of laboratory experiments that exposed artificial mussel beds to distinct hydrodynamic conditions (water flow and wave splash) and field assessments of natural beds, we tested the hypothesis that microplastic accumulation and ingestion are higher in beds composed of highly eroded mussels compared to beds of non-eroded conspecifics.

2. Methods

2.1. Field assessment of plastic trapping

Plastic trapping in infested and non-infested mussel beds naturally occurring on rocky shores was evaluated by collecting patches of *Mytilus galloprovincialis* (15 cm in diameter; $n = 6$ for each treatment; Plettenberg Bay 34.005°S, 23.45°E, South Africa), including their basal matrix of sediment, and byssal threads from beds in the mid mussel zone. Collections were made during the a single low tide using a metal scraper and only cotton clothes were worn. Immediately after collection, samples were brought in glass containers to the laboratory where each sample was treated in order to quantify microplastics (a) in the sediment matrix, (b) on the surface of mussel shells, (c) ingested by individual mussels. Microplastic (MP) identification was done using the Guide to Microplastic Identification (MERI, 2015). Following the Guide, particles that did not break or dissolve when pressed with tweezers were classified as MPs. MP items were counted, photographed and measured using the software Image J (https://imagej.nih.gov/ij/index.html; Schneider et al., 2012). The particles were categorised according to their shape (fragment, fibre, film, foam, or microbead; Gündoğdu and Çevik, 2017) and size class (using1 mm intervals). At the end of all experiments, mussels from each sampled bed were measured for length and categorised by shell length (0–1 mm, 1–2 mm, 2–3 mm, 4–5 mm, and 5–6 mm) and level of infestation defined as A - non-infested, B, C, D, E - severely infested following Zardi et al. (2009).

2.1.1. Sediment matrix

MPs were extracted from the matrix of sediment and byssal threads by density separation (Hidalgo-Ruz et al., 2012), using a filtered hypersaline

solution prepared with ultrapure water (350 g NaCl L-1). Each sample (n = 6) was transferred into a glass jar (3.3 L) containing 2 L of the hypersaline solution, mixed for 3 min using a metal spoon and then allowed to settle for 1 h. After sedimentation, ca. 2.5 L of the overlying water was filtered through a GF/C Whatman filter (47 mm of diameter, 1.2 μm of pore size) using a glass vacuum system. When necessary, several filters were used to avoid clogging. Mixing and filtering were done twice for each sample to allow the flotation of denser polymers and plastic particles potentially trapped by organic matter (e.g., Hidalgo-Ruz et al., 2012; Mathalon and Hill, 2014). Filters were then placed in pre-labelled glass petri dishes and dried (40 °C, 24 h), followed by visual examination under a stereomicroscope (Leica S8 APO, x40). MPs were visually identified, counted and categorised as described above. Each sample was then sieved (500 μm), dried in an oven at 70 °C to constant weight and weighed to the nearest 0.001 g. MP abundance was expressed as number of items g^{-1} of sediment DW.

2.1.2. Mussel shells

From each sampled bed (n = 6), three individual mussels (3–5 cm in shell length) were set aside to assess MP ingestion. All the remaining mussels from the bed were placed in a 3.3 L glass jar where MPs were extracted by density separation and visually identified, counted and categorised as described above. Mussels (shell and soft tissue) were then dried in an oven to constant weight at 70 °C and weighed to the nearest 0.001 g. MP abundance was expressed as number of items per g^{-1} of mussels DW.

2.1.3. Extraction of MP in individual mussels

Wet soft bodyweight (g WW) was measured using a microbalance (0.001 g precision). Individuals in each sample were rinsed with pre-filtered tap water (tap water filtered through a GF/C Whatman with 1.2 μm pore size) to remove potential external contaminants adhered to the shells. Shells were opened, and soft tissue was extracted and weighed (g WW) to the nearest 0.001 g, then rinsed again with pre-filtered tap water. The whole soft tissue was used as an effective method to assess plastic pollution in the field and as a relative comparison of mussel ingestion between treatments. MP extractions were subsequently conducted in a laminar flow cabinet using an adapted protocol from Dehaut et al. (2016). Each composite sample (i.e. made up of 3 mussels) was placed in a 250 mL flask and 1.8 M KOH solution was added to digest the organic matter. The solution was stirred for 2 min to complete digestion and placed on a hot plate stirrer set at 60 °C and 1000 rpm for 24 h. After incubation, the whole solution was filtered through a Whatman GF/C glass-fibre filter (diameter 47 mm, 1.2 μm pore size) while still warm, using a glass vacuum system. The resulting filters were placed in glass petri dishes with lids, dried in the oven at 40 °C for 24 h, then examined for the presence of MPs as described above. MP abundance was expressed as number of items per wet soft-tissue weight (items g^{-1} WW).

2.1.4. Quality control

To eliminate post-sampling contamination, gloves and 100% cotton laboratory coats were throughout worn during the laboratory treatment process. In addition, all equipment used was non-plastic (i.e., glass or metal), and was rinsed twice with pre-filtered ultrapure water between sample extractions. Aluminium foil was used to cover material before use and to cover glass jars during settling intervals and while filtering. To account for potential contamination, one procedural (blank) control (containing KOH solution only for extraction in mussels or hypersaline solution only for sediment and shells) was performed in parallel to each batch (i.e., each batch was made up of 1 control and 1 of each of the two treatments), yielding an average procedural MP contamination of 0.66 ± 0.82 items in 250 ml of solution (mean ± standard deviation, SD) for extraction in mussels, 0.5 ± 0.55 in 3.3 l of solution (mean ± SD) for sediment matrix and 0.17 ± 0.41 in 3.3 l solution (mean ± SD) for mussel shells.

2.1.5. Polymer identification

To obtain information on polymer composition and to validate MP identification, FTIR microspectroscopy was used. IR-ATR spectra between 500 cm^{-1} to 3500 cm^{-1} were collected using a Nicolet iN10 Fourier infrared microspectroscopy (Thermal Fisher Scientific Co., USA). Micro Tip ATR was placed in contact with the sample to record the spectra, with air as the background spectrum. Recorded spectra were compared against commercial FTIR spectral libraries (Hummel Polymer and Additives Library and FBI fibre library).

2.1.6. Data analyses

Differences in frequency distributions of mussel size classes between infested and non-infested beds were assessed using a Chi-squared Test of Independence. The effect of infestation on plastic trapping by mussel beds was analysed in two ways. First, MP abundance across plastic categories was calculated and used in a series of Kruskal-Wallis tests with treatment (2 levels; infested, non-infested) as the factor and overall counts of MPs in the sediment matrix, on mussel shell or ingested by mussels as the dependent variable. Second, data were tested for the effects of treatment on the proportions of different plastic polymers in mussels, in sediment or on mussel shells. To do this, a series of 1-way multivariate PERMANOVA tests were performed with treatment (2 levels; infested, non-infested) as a fixed factor and abundance of each polymer as the dependent variable. Each analysis was run with 9999 permutations using Bray–Curtis dissimilarity matrices (Clarke et al., 2006) for square-root transformed multivariate measures (Anderson, 2006). To represent each dataset visually, a two-dimensional non-metric multidimensional scaling plot (MDS) was used. All multivariate analyses were performed using PRIMER 6.1.15 and PERMANOVA + 1.0.5 software (Clarke and Gorley, 2006).

2.2. Laboratory experiments

To simulate the various hydrodynamic conditions experienced by a mussel bed over the course of a tidal cycle, we designed two sets of experiments where mussel beds would experience (*i*) the kinetic energy of water flowing over them when immersed during high tide and (*ii*) the kinetic energy of breaking waves while emerged. These experiments are referred to hereafter as flow and wave splash experiments respectively.

All experiments were run using artificial mussel beds made of either non-infested or infested biomimetic mussels as the primary treatment. Biomimetic mussels were constructed by replacing the tissues of mussels with silicon and used to artificially create mussel beds (Lourenço et al., 2017b). Based on previous categorization of endolithic infestation (Zardi et al., 2009), infested beds were made of mussels belonging to the infestation categories C and D, while non-infested beds were made up of non-infested mussels (i.e., category A). These beds were circular (ca. 20 cm in diameter) and made of mussels (5 ± 0.5 cm in length; n ~ 55–65 mussels per bed) arranged vertically to mimic their position in natural beds (Fig. S1). Semi-rigid, white PVC net (mesh size 1 cm) was placed around the beds to keep the mussels in position while a soft substratum was placed underneath the nets in order to simulate the complex soft matrix of organic matter, shell debris and sediment characterizing the basal layer of natural mussel aggregations.

2.2.1. Flow experiment

To simulate the free stream velocities occurring above intertidal beds at high tide, we created a steady unidirectional flow in a 30-cm wide smoothed-wall recirculating flume (2 m long by 1 m wide; Fig. S2) filled with 30 cm of seawater (33 PSU), where artificial mussel beds were individually placed in the middle of a 1-m-long linear section. Water was entrained by surface friction through the rotation of a set of 10 vertical PVC disks (60 cm diameter, 5 mm thick) and set up at three flow rates corresponding to free-stream velocities U_F over the flat flume bottom in front of the mussel bed (U_F = 0.11, 0.38 and 0.63 $m.s^{-1}$), and over the mussel bed (U_B = 0.13, 0.47 and 0.81 $m\ s^{-1}$). These velocities are referred to as slow, medium and high flow velocity hereafter. The increase observed between U_F and U_B is induced by the presence of the mussel beds, which leads to accelerated flow due to the reduction in channel cross-sectional area over the mussel bed. These figures are consistent with previous estimates of 20 to 27%

flow acceleration over a mussel bed height of 6.1 cm maintained in 40 cm of water in a 60 cm wide flume under free-stream velocities U_F of 0.045, 0.10 and 0.27 m.s^{-1} (van Duren et al., 2006). The flume was calibrated using the ensemble average velocity of the speed of a drifter over the linear section of the flume. This surface velocity correlates linearly with the rotation speed of the wheels. Preliminary experiments showed that the free stream velocity did not differ significantly over the width or depth of the linear section of the flume where the artificial mussel beds were deployed (unpublished data; see also Seuront et al., 2001, Seuront et al., 2004, Seuront and Schmitt, 2005b for further details on the turbulent properties of the flow generated in this flume, Seuront and Schmitt, 2005a).

The velocity profile $u(z)$ above the mussel bed was recorded every 5 mm for 10 s using an Acoustic Doppler Velocimeter (ADV; Vectrino Plus, Nortek AS) at a frequency of 200 Hz. In the coordinate system of the carriage, x was defined as the direction along the main flow direction, y across the flume channel and z the vertical direction. We defined $z = 0$ to be the average height of the mussel bed determined as 5.5 cm using the distance-to-boundary function of the ADV to determine the height of the mussel bed at several locations. No significant differences were found in bed height between non-infested and infested beds (Kruskal-Wallis test, $p > 0.05$). Each profile contained 31 points, the highest one at 150 mm above the bed. In addition to the profiles over the mussel beds, three profiles were collected at each of the three experimental velocities over the flat PVC bottom surface ca. 15 cm upstream of the location of the artificial mussel beds. The velocity profile $u(z)$ is typically expressed as the so-called law of the wall (Mann and Lazier, 1991):

$$u(z) = (u_* / \kappa) \ln (z/z_0) \quad (1)$$

where κ is the Von Kármán constant ($\kappa = 0.41$), and z the distance above the mussel bed. From Eq. (1), it is readily seen that the roughness length z_0 (m) and the shear velocity u_* (m.s^{-1}) can respectively be estimated as the z-intercept and the slope of a plot of $u(z)$ vs. ln(z). The bed shear stress τ_0 (Pa) was subsequently estimated as $\tau_0 = \rho u_*^2$, where ρ is the density of seawater. Eq. (1) is based on the assumption that within the benthic boundary layer the velocity gradient is shaped by friction drag, and thus it does not hold when (i) the boundary layer is dominated by viscous forces and/or (ii) the roughness elements (e.g., sediment grains or biogenic structures) are large enough to generate turbulent wake structures. Very close to the bottom and when roughness elements are relatively small, viscous forces dominate. In this region, referred to as the viscous sublayer (VSL), the velocity $u(z)$ is a linear function of z, u_* and the kinematic viscosity n as $u(z) = zu_*^2/\nu$ INCLUDEPICTURE "D:\\var\\folders\\w3\\61j5ws953mg4kpv3yz3t3_x00000gn\\T\\com.microsoft.Word\\WebArchiveCopyPasteTempFiles\\0?ui=2&ik=31543399dc&attid=0.1.1&permmsgid=msg-f1722865660295031849&th=17e8d9309d9aac29&view=fimg&fur=ip&sz=s0-l75-ft&attbid=ANGjdJ8VBVliyb-5zUOfCx_6-BSKcRqihWmmAW3FevT6hrAGIjDsX3R1Yxd15XQI6rsCH4v57-MRHCs0XacibeVfWusq-1hD7V-fA4qLEBDuBjan4YVb6a8i-TSYruE&disp=emb" * MERGEFORMAT. In the VSL, which is about $12n/u_*$ thick, the flow is hydraulically smooth, but when the flow is strong enough and/or the bottom rough enough, the flow becomes 'hydraulically rough' and the VSL is only present in the interstices of the bed. In turn, when roughness elements increase in size, and form turbulent wakes, drag starts to play a role (Arya, 1975; Chriss and Caldwell, 1982), which can lead to the formation of several internal boundary layers, each with a different shear velocity u_*, as previously shown in flume tanks over a periphyton mat (Nikora et al., 1997) and a bed of the mussel *Mytilus edulis* (Van Duren et al., 2006) and in the field over beds of the horse mussel *Atrina zelandica* (Nikora et al., 2002). The lower logarithmic layer was referred to as the 'near-bed roughness sublayer' (Nikora et al., 1997) and the two logarithmic layers found over a *M. edulis* bed as the 'higher and lower boundary layers' (Van Duren et al., 2006).

Turbulent kinetic energy (TKE) (ε) was estimated at each distance z above the mussel bed as $TKE_{(Flow)} \leq w>^2/2$ (Denny and Shibata, 1989), where w is the root-mean-square turbulent velocity fluctuation estimated as the sum of the variances of the three-dimensional turbulent velocity components u', v' and w', i.e. $w = \left(\overline{(u\prime)^2} + \overline{(v\prime)^2} + \overline{(w\prime)^2}\right)^{0.5}$. The turbulent velocity components are defined as the difference between the instantaneous and average velocities, i.e., $u' = u - \overline{u}$, $v' = v - \overline{v}$ and $w' = w - \overline{w}$, with $\overline{(u')^2} = \frac{1}{n}\int_1^n (v_x - \overline{v_x})^2$, $\overline{(v')^2} = \frac{1}{n}\int_1^n (v_y - \overline{v_y})^2$ and $\overline{(w\prime)^2} = \frac{1}{n}\int_1^n (v_z - \overline{v_z})^2$. The Reynolds shear stress τ (Pa), $\tau = -\rho\overline{u\prime w\prime}$, which, under the assumption that the rates of transport of momentum and mass are identical (Rutherford, 1994; Monin and Yaglom, 2013), determines the vertical transfer of mass to the bottom (i.e., the transport of mass from one volume of fluid to another induced by turbulent velocity fluctuations) was also calculated to assess the link between turbulent stress and mussel bed roughness.

For each stream velocity (0.13, 0.47 and 0.81 cm s^{-1}) and treatment (non-infested and infested mussel beds), three trials were run with different beds ($n = 3$). Each trial consisted of running the entrainment system for an initial 5 min to establish a steady unidirectional flow. Subsequently, the flume water was loaded with MPs of 1 mm in length at a concentration of 2.95 g l^{-1} of seawater, and the flow experiment run for 10 min. The entrainment flow was then stopped and after 5 min, when the flow was nil, both the mussel bed and its basal layer were carefully removed, rinsed separately with freshwater over a 1 mm pore size sieve. The collected MPs were dried at 60 °C for 12 h and weighed to the nearest 0.0001 g.

2.2.2. Wave splash experiment

The effect of wave splash on mussel beds was simulated pouring a volume of water V (l) from a height h (m) on an emerged artificial mussel bed to simulate wave action. By virtue of the law of the conservation of energy, which states that the potential energy of a falling object equals the kinetic energy of the object upon impact with a substratum, the resulting kinetic energy of the 'wave splash' was estimated following Meriam et al. (2020) as $\varepsilon_{(WaveSplash)} = mhg$ (J), where m is the mass of the volume of water V (i.e., $m = dV$, where d is the density of seawater at a temperature of 25 °C and a salinity of 35 PSU, i.e., 1.0236 kg.l^{-1}), and g the gravitational acceleration ($g = 9.81$ m.s^{-2}). Using two different volumes of seawater to simulate weak ($V = 0.5$ l) and strong ($V = 5$ l) wave action, the resulting kinetic energy was respectively 15.1 and 1.5 J; these two volumes of seawater were specifically chosen to simulate the hydrodynamic effects induced by weak and strong wave conditions respectively. Each simulated wave was homogenously loaded with MPs at a concentration of 2.95 g l^{-1} of seawater. MP particles consisted of fragments of 1 mm in length.

Each splash experiment consisted of simulating one wave (weak or strong) on one bed treatment (non-infested or infested) after which, MP particles were collected from the mussel bed and its basal layer separately by rinsing each section with freshwater over a 1 mm pore size sieve. The collected MPs were then dried at 60 °C for 12 h and weighed to the nearest 0.0001 g. For each treatment and wave strength, the splash experiment was carried out 3 times ($n = 3$).

2.2.3. Data analyses

The effect of infestation on plastic trapping during high tide was assessed with a 3-way ANOVA with treatment (2 levels: infested, non-infested), flow strength (3 levels: high, mid, low) and position (2 levels: base, mussel bed) as fixed factors and the weight of trapped MPs as the dependent variable.

The effect of infestation on mussel bed trapping at low tide, after initial wave splash of incoming tides, was assessed with a 2-way ANOVA with treatment (2 levels: infested, non-infested) and position (2 levels: base, mussel bed) as fixed factors and the weight of trapped MPs as the dependent variable. Each wave strength (strong and weak) was analysed separately and not included as an additional factor as data failed the test for homogeneity of variance (Levene's test) even after square root or logarithmic transformation.

2.3. Rugosity assessment

We further investigated the rugosity of the mussel beds through an assessment of the complexity of the bed surface using fractal analysis (Commito and Rusignuolo, 2000). Mussel beds are fundamentally composed of multiple copies of individual mussels of different sizes but similar shape, i.e., a mussel bed can theoretically be decomposed into multiple re-scaled copies of one large mussel, down to the smallest possible mussel. As such, mussel beds are a perfect candidate for exhibiting self-similarity, a property quantified through fractal analysis (e.g., Sugihara and May, 1990; Seuront, 2010). Fractal analysis identifies self-similar properties across scales and, in our case, we expect endolithic infestation to increase the surface complexity of a mussel bed. Fractal dimensions, D, are estimated by superimposing a regular grid of squares of size l on a given object and counting the number of 'occupied' squares. This procedure is repeated using different values for l, allowing the surface occupied by the object to be estimated with a series of counting squares spanning a range of surfaces down to some small fraction of the entire surface. The number of occupied squares increases with decreasing square size, leading to the following power-law relationship:

$$N(l) = kl^{-D} \tag{2}$$

where l is the square size, $N(l)$ the number of squares occupied by the object and D is the so-called fractal dimension.

Here, the rugosity of both non-infested and infested mussel beds was assessed from the complexity of the bed surface contours (Fig. 1A,B). Even though our experimental beds consisted of relatively tightly packed mussels of similar size, their surface is typically irregularly shaped, with gaps, invaginations and evaginations that are expected to have a relatively smooth surface with a small fractal dimension. Because even slight reorientation of a mussel bed can produce different values of $N(l)$, hence potentially modify the complexity of its surface as estimated by the fractal dimension D, the surface complexity of each individual mussel bed was analysed from 18 pictures taken from successive angles with 10° increments from 0 to 170°. This procedure also allows the detection of potential lack of isotropy in our artificial mussel beds (Katrak et al., 2008, Seuront, 2010 for details). The presence of differences between the resulting fractal dimensions (D_i) was inferred using an analysis of covariance (Zar, 1999). In the absence of significant differences among these intermediate fractal dimensions D_i, the surface complexity of a mussel bed was quantified as $D = \sum_{i=1}^{18} D_i$. Because an objective procedure is needed to identify the appropriate range of scales l to include in the regression analysis of the log-log plots of $N(l)$ vs. l, we considered a regression window of varying width ranging from a minimum of 5 data points to the entire data set. The smallest windows are slid along the entire data set at the smallest available increments, with the whole procedure iterated $n - 4$ times, where n is the total number of available data points. Within each window and for each width, we estimated the coefficient of determination (r^2) and the sum of the squared residuals for the regression. We subsequently used the values of l (Eq. (2)), which maximized the coefficient of determination and minimized the total sum of the squared residuals (Seuront, 2010), to define the scaling range and to estimate the related dimensions D_i.

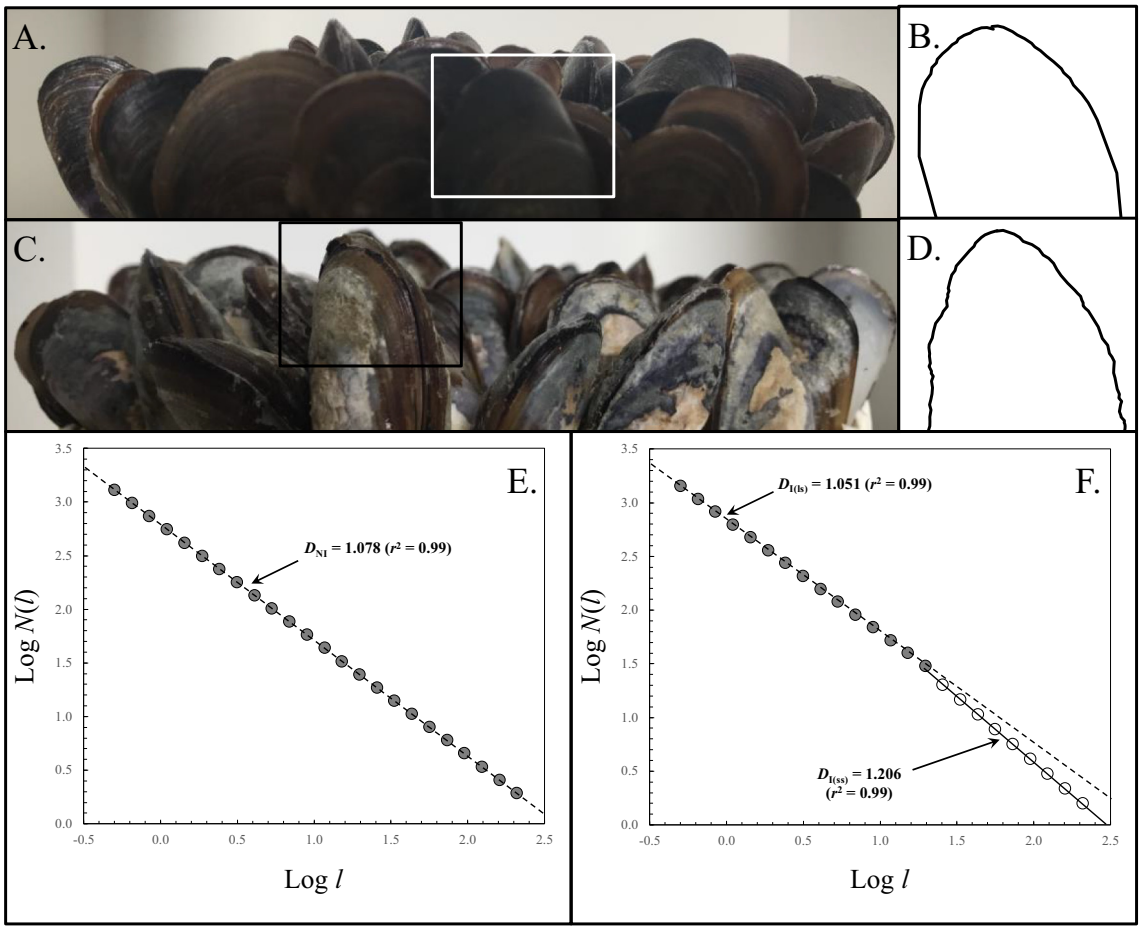

Fig. 1. Non-infested (A) and infested (C) mussel beds, with close-up on the typical surface topography of a non-infested mussel (B) and an infested mussel (D). The results of fractal analysis are shown as typical log-log plots of $N(l)$ vs. l, for non-infested (E) and infested (F) beds. Non-infested beds exhibit a very strong scaling range over the whole range of scales considered (i.e., 0.5 to 200 mm), with the resulting fractal dimensions ranging from 1.06 to 1.09. In contrast, infested beds were characterized by two distinct scaling ranges occurring for scales ranging from 0.5 to 20 mm and 20 to 200 mm, with significantly different fractal dimensions respectively ranging from 1.17–1.22 and 1.05–1.08, respectively.

3. Results

3.1. Field assessment of plastic trapping

No association was found between mussel size class distribution and treatment (X2(2) = 1.186, p = 0.553). Only fibres and fragments were recorded in natural beds. Specifically, only fibres were ingested by mussels, while this category represented 41.6% and 83.3% of all MPs found in the sediment matrix and on mussel shells respectively. On average, more plastic was ingested than trapped in shells or sediment matrix. MPs were significantly more abundant in infested than in non-infested treatments (Fig. 2B-D; H2 = 5.067, p = 0.024 for shell trapping; H2 = 8.308, p = 0.004 for sediment matrix trapping; H2 = 8.307, p = 0.004 for mussels). The pattern in the polymer counts did not differ between treatments for ingested MPs (PERMANOVA, Treatment, p(Perm) = 0.447; Table S1; Fig. S3), those retained by the sediment matrix (PERMANOVA, Treatment, p(Perm) = 0.917) or those trapped on mussel shells (PERMANOVA, Treatment, p(Perm) = 0.058).

3.2. Rugosity assessment

Non-infested beds (Fig. 1A,C) were consistently characterized by a very strong linear behaviour of log–log plots of $N(l)$ vs. l over the whole range of available scales (i.e., from 0.5 to 200 mm; Fig. 1E) with coefficients of determination (r^2) ranging from 0.98 to 0.99. For each mussel bed, no significant differences were found between the resulting intermediate fractal dimensions D_i ($p > 0.05$) which confirms the isotropic nature of our mussel beds. The resulting fractal dimension for non-infested beds (D_{NI}), ranged from 1.06 to 1.09 and did not significantly differ among our three experimental beds (p > 0.05). In contrast, infested beds (Fig. 1B,D) were characterized by two distinct power-law behaviours at scales smaller and larger than 20 mm (Fig. 1F). No significant differences were found between the intermediate fractal dimensions D_i within each bed, nor between beds for each scaling range. The surface complexity of infested beds differed, however, between scaling ranges (Student's t-test, $p < 0.01$; Zar, 1999), with the resulting fractal dimensions D_I being significantly higher at the small scale, i.e. 0.5 to 20 mm ($D_{I(ss)} \in [1.17–1.22]$; an increase in complexity of ca.15%) than at the larger scale, i.e. 20 to 200 mm, ($D_{I(ls)} \in [1.05–1.08]$). Noticeably, no significant differences were found between D_{NI} and $D_{I(ls)}$, which suggests that endolithic infestation only modifies surface complexity at scales characteristic of individual mussels.

3.3. Laboratory experiments

3.3.1. Hydrodynamic properties of flow over mussel beds

The vertical structure of the flow velocity observed over the flat bottom of the tank upstream from the mussel beds was highly significantly (r^2 = 0.99, $p < 0.001$) and was described by a unique logarithmic layer, indicating an ideal boundary layer over the whole range of distances from the bottom considered here, i.e. from 0.5 to 155 mm (Fig. S4, Table S2); this observation implies that the flow velocity $u(z)$ increases as a logarithmic function of the distance z from the bottom of the tank, see Eq. (1). In contrast, the flows observed over both non-infested and infested *M. edulis* beds were far more complex. They did not show a unique logarithmic layer, as expected over smooth surfaces (Chriss and Caldwell, 1982; Nikora et al., 1997; Nikora et al., 2002; Van Duren et al., 2006). Instead, they were consistently characterized by an internal boundary layer of varying thickness, and an upper layer separated by a clear break occurring in the scaling of $u(z)$ vs. ln(z); see Fig. S4 and Table S2. The thickness of the internal boundary layer significantly increased with the free-stream velocity U_B with $\delta_{slow} < \delta_{medium} < \delta_{fast}$ for both non-infested and infested mussel beds (Table S2). Noticeably, the friction velocity u_*, which consistently increased with U_B over both non-infested and infested beds, was consistently significantly higher (Student's t-test, $p < 0.01$) over infested mussels. This result indicates a steeper velocity gradient over infested mussels than over non-infested mussel beds. Note that δ was consistently significantly thicker over infested beds, irrespective of U_B (Table S2). Each velocity profile was subsequently characterized by a lower and an upper layer, with properties clearly dependent on both the free-stream velocity and the infestation of the mussels (Fig. S4, Table S2).

The friction velocity u_*, roughness length z_0, the bed shear stress τ_0, and turbulent kinetic energy (TKE) were consistently significantly higher

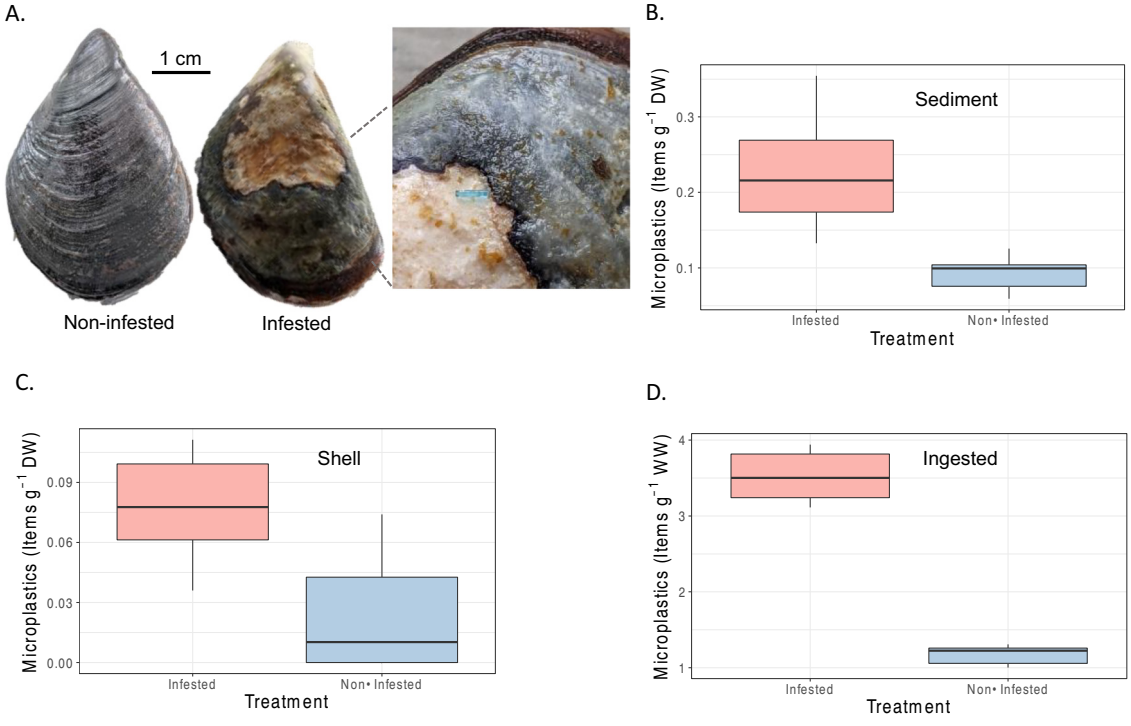

Fig. 2. (A) Example of infested and non-infested mussels and close up of the infested individual with a trapped microfiber. Box-plots of the overall MP abundance in infested and non-infested mussel beds (B) in the sediment matrix, (C) on mussel shells, (D) ingested by mussels.

within the internal boundary layer occurring over infested than non-infested beds. The relative difference between non-infested and infested beds decreased with free-stream velocity U_B for u_* (29–34% at 130 mm s^{-1}, 15–20% at 470 mm s^{-1}, and 8–12% at 810 mm s^{-1}), z_0 (ca. 4-fold at 130 mm s^{-1}, 3.5-fold at 470 mm s^{-1}, and 2-fold at 810 mm s^{-1}) and τ_0 (66–79% at 130 mm s^{-1}, 31–44% at 470 mm s^{-1}, and 16–25% at 810 mm s^{-1}). In contrast, turbulent kinetic energy (TKE) noticeably increased with free-stream velocity by ca. 80%, 106% and 240% at 130 mm s^{-1}, 470 mm s^{-1}, and 810 mm s^{-1}, respectively. The Reynolds stress τ was significantly stronger (i.e., 39 to 48%) in the internal boundary layer overlying infested beds at 130 mm s^{-1}, but this difference became non-significant at 470 mm s^{-1}, and 810 mm s^{-1} ($p > 0.05$). Finally, TKE and Reynolds stress ($\tau = -\rho\overline{u'w'}$) were consistently significantly weaker in the lower than in the upper layer (Table S2).

3.3.2. Plastic trapping

Under simulated high tide conditions, infestation had a significant effect on MP trapping by mussel beds but the effects differed among layers of the beds and among stream velocities (Fig. 3A-C; 3-way ANOVA; sqrt-transformed; Treatment x Position x Flow: $F_{2,24} = 6.56$, $p = 0.005$).

Specifically, on shells, the infested treatment trapped more MPs than non-infested patches (SNK test: $p < 0.001$) while, overall, fewer MPs were trapped under high flow than reduced velocities (i.e., High < Mid = Low; $p < 0.001$). At the base, infested beds trapped fewer MPs than non-infested patches at low velocities (SNK test: $p = 0.016$), with no treatment effect at mid or high flow velocities ($p = 0.105$ and $p = 0.328$ respectively). More generally, the base of the bed retained more MPs (on average 79% more) than mussel shells.

Under simulation of both strong and reduced wave intensities, infested mussel beds trapped more MPs than non-infested mussel ones (Fig. 4; 2-way ANOVA; Treatment: $F_{1,8} = 13.27$ and $F_{1,8} = 51.57$ respectively, $p < 0.001$ in both cases) and more MPs were found on the upper part than on the understory of the bed (Position: $F_{1,8} = 36.66$ and $F_{1,8} = 30.34$ respectively, $p < 0.001$ in both cases).

4. Discussion

In this study, we demonstrate that symbiont-induced intraspecific, phenotypic variation in the physical properties of mussel beds alters flow dynamics and MP trapping and retention, leading to changes in the passive delivery of MPs to mussels for consumption.

Our assessment of the surface complexity of non-infested and infested beds shows that endolithic infestation only affected surface complexity at scales smaller than individual mussels. Nevertheless, the ca. 15% increase in surface complexity over these small scales induced major consequences on the hydrodynamic properties of the flows overlaying beds, particularly in terms of the roughness length (which was increased by infestation by 2- to 4-fold depending on flow velocity) and the subsequent generation of microscale turbulence and modification of near-bed velocity profiles. These results support previous research on a range of fluid dynamics assessed over artificial surfaces of different rugosities (Krogstadt and Antonia, 1999; Bergstrom et al., 2002) and over biogenic surfaces (Butman et al., 1994; Nikora et al., 1997; Nikora et al., 2002; Van Duren et al., 2006; Drobnitch et al., 2017).

The higher quantity of MPs accumulating on the shells of infested mussels irrespective of free-stream velocity is consistent with the significantly larger velocity gradient, the larger roughness length and the stronger turbulent kinetic energy observed in the internal boundary layer overlying infested beds. In particular, the combination of reduced flow and increased turbulence are consistent with higher encounter rates between non-motile objects (here mussels) and MP particles freely advected by turbulent velocity fluctuations within a thicker boundary layer. This encounter rate is a direct function of the root-mean-square turbulent velocity w (e.g., Evans, 1989) which scales as $TKE^{0.5}$. As such, the 80%, 106% and 240% relative differences observed between the TKE measured in the internal boundary layer overlying non-infested and infested beds lead to a 1.3- to 1.8-fold increase in w and hence in encounter rates. These figures are compatible with the 1.6 to 1.8-fold increase in the quantity of plastic found on infested mussels compared to non-infested individuals. Likewise, the quantity of MP particles trapped within mussel beds is in line with the related differences observed in the friction velocity τ_0 and the Reynolds shear stress τ (Table S2). At the smallest free-stream velocity, the bed shear stress τ_0 was comparable to the critical bottom shear stress reported in the literature

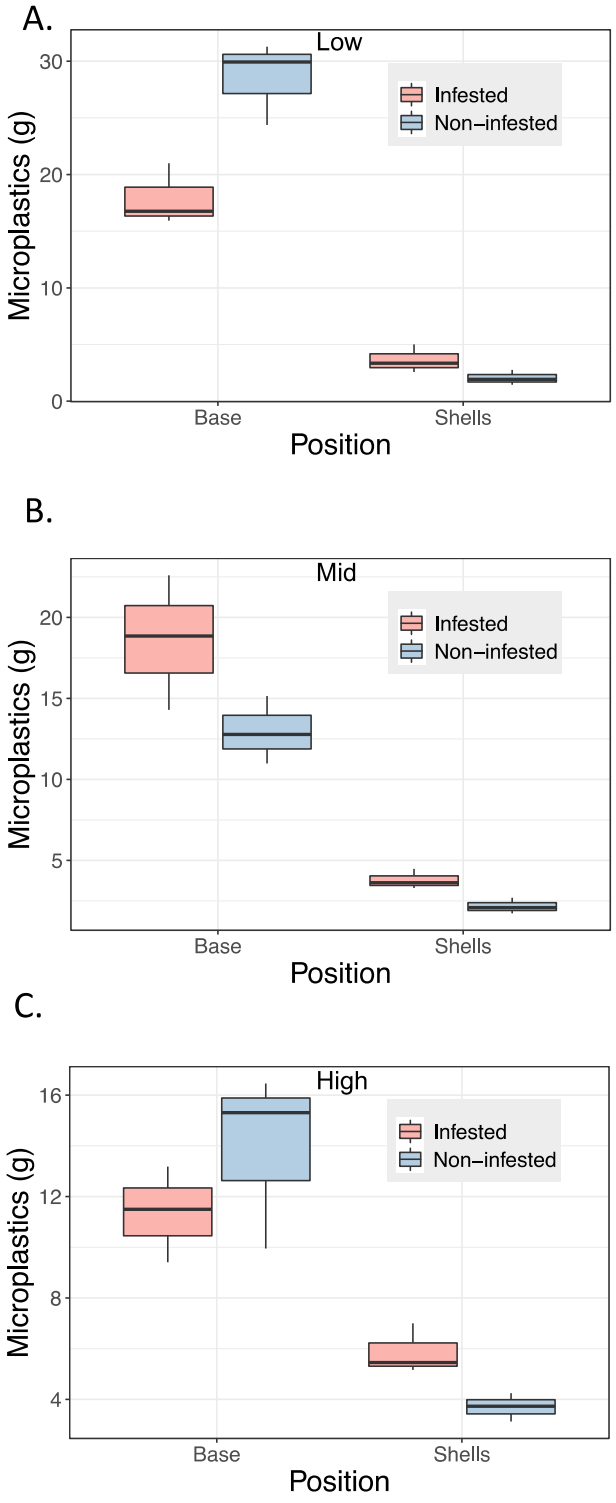

Fig. 3. Flow experiment. Box-plots of the weight of MPs trapped by infested and non-infested mussel beds during high tide at (A) low, (B) mid and (C) high water velocities.

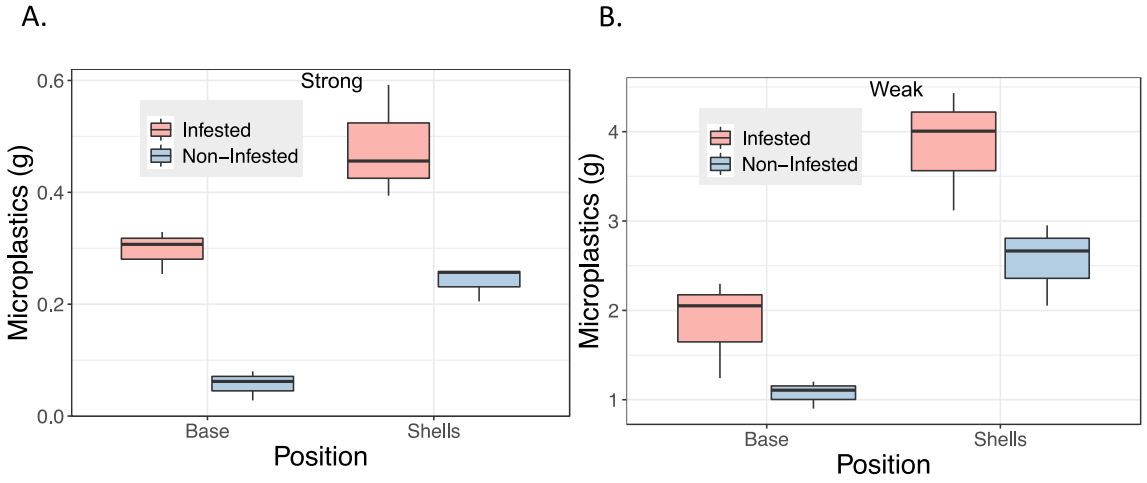

Fig. 4. Wave splash experiment. Box-plots of the weight of MPs trapped by infested and non-infested mussel beds after the splash of waves at incoming tide for (A) strong wave and (B) weak wave conditions.

for resuspension of sediment (i.e., 0.10–0.14 Pa; Wright et al., 1997) and particulate matter (i.e., 0.13 Pa; Burchard and Baumert, 1998). These observations, coupled with the significantly higher Reynolds stress observed over non-infested beds compared to infested ones, indicate higher MP transport towards the bottom with very limited possibility of resuspension. In contrast, the drastic increase in friction velocity (τ_0) observed at intermediate and high velocities is likely to favour resuspension, explaining both the decrease in plastic retention and lack of significant differences between the retention observed in infested and non-infested beds when they were exposed to higher flow velocities. This interpretation is supported by the lack of significant difference in Reynolds stress over infested and non-infested beds under higher flow. Nevertheless, regardless of the different retention and trapping processes suggested above, the observed increase in plastic retention on infested mussel shells and within infested beds is in accordance with the role of increased turbulence in the retention of MP particles at the surface of mussels with greater shell rugosity, and suggests that the complex surface structure of mussel beds may play a role in trapping MP particles through a massive increase in vertical transport. The spatial resolution of this specific issue lies well beyond the scope of the present work, and would require measurements of the nature of the flow above and within non-infested and infested mussel beds following wave exposure.

Critically, in nature, water flow and wave action can be extremely variable both in time and in space (e.g., Denny, 1995; Zardi et al., 2006; Nicastro et al., 2008; Denny and Gaylord, 2010). Hydrodynamic variation within the intertidal is well known to play a key role in supplying nutrients and sediment and the breaking or dislodgement of organisms, thus helping determine the structure and dynamics of many communities in intertidal systems (e.g., Menge, 1976; Paine and Levin, 1981; Sousa, 1984). Our findings indicate that spatio-temporal variation in the frequency and intensity of water flow and waves could significantly affect the magnitude of plastic trapping along hydrodynamic gradients. Such effects can be either direct, through the transport of plastics to or from mussel aggregations, or indirect by influencing the frequency of endolithic infestation through the removal the periostracum of shells, a precondition of endolithic infestation (Kaehler, 1999; Ndhlovu et al., 2020).

Furthermore, regardless of flow intensity, our results from laboratory high tide simulations matched field results, revealing significantly higher amounts of plastic at the base of the mussel beds than on the shells. This is in line with previous field work assessing plastic accumulation in coastal vegetated habitats dominated by canopy-forming bioengineers (Cozzolino et al., 2020). Despite high variability in plastic trapping, which is largely dependent on habitat and position on the shore, MPs persistently accumulate more on the surface of sediments than in the vegetative canopy (Cozzolino et al., 2020). In contrast, in the simulation of incoming waves, we found that more MPs were trapped on shells than at the base of the mussel aggregation. Given the pattern observed in the field, this suggest that it is a transitory condition for both infested and non-infested beds where most of the particles trapped on the shell are eventually transported at the basal section of the bed. Future experiments testing how microplastic sedimentation varies through time, could confirm this suggestion.

Endolith-induced corrosion is a wide-spread phenomena in intertidal ecosystems. Microbial endoliths that degrade mussel shells have been reported in multiple bioregions, ranging from cold-temperate to subtropical/tropical conditions (Ndhlovu et al., 2019). Their corrosive activities are modulated by varying environmental conditions across large to small spatial scales and are generally related to gradients in solar radiation, hydrodynamic stress and wind stress (Kaehler, 1999; Zardi et al., 2009). For instance, endolithic corrosion increases with wave exposure (Zardi et al., 2016; Ndhlovu et al., 2020); the physical damage to the outer shielding periostracum of mussels caused by abrasion by wave- or wind-borne sand facilitates the initial stages of endolithic shell excavation (Kaehler, 1999). At smaller spatial scales within the intertidal, variation in light exposure affects the distribution of photoautotrophic endoliths thus causing more intense shell corrosion at non-shaded sites. The determinant role of light is also visible at geographic scales. A large-scale survey along the Atlantic shores of Portugal, Morocco and Western Sahara, revealed higher incidences of phototrophic shell-degrading endoliths at lower latitudes that correlated with higher solar radiation and lower cloud cover (Lourenço et al., 2017b). In the context of plastic pollution, this suggests that the incidence of endolith-induced corrosion in mussel beds is likely to be a determinant of topographic changes in MP retention in these biogenic habitats. Characterizing such variation is, therefore, necessary to understand the dynamics of MP accumulation, and to develop targeted management strategies.

Our results indicate the complexity and context dependency of the relationship between endoliths and their hosts. Endoliths cause distinctive whitening of mussel shells leading to reduced uptake of solar energy and heat stress (Zardi et al., 2016, 2021), which is likely to be increasingly beneficial as heatwave frequency, duration and cumulative heat are projected to increase (Perkins-Kirkpatrick and Lewis, 2020). Nevertheless, the relationship is generally negative from the host perspective. The conspicuous amount of energy used to repair the shell alters the energetic budgeting of mussels and comes at the expense of other processes such as growth, reproduction and strength of byssal attachment (Zardi et al., 2009; Ndhlovu et al., 2021). Here, we show that symbiotic microbes can also amplify the negative effects of another anthropogenic stress, plastic pollution. Increased retention and accumulation of MPs by the mussel biogenic habitat is likely to increase the bioavailability and ingestion of MP (e.g., Piarulli and Airoldi, 2020), trophic transfer (e.g., Zhao et al., 2018), and plastic leachate-induced behavioural changes (e.g., Seuront et al., 2020) among species associated with these habitats.

Critically, intertidal mussels are multitasking ecosystem engineers crucial for the maintenance of local biodiversity (Jones et al., 1994). For instance, evidence from the NE Pacific and the South African coast shows that 10s to 100 s of species (e.g. invertebrates, small fish and seaweeds) depend on mussel beds (Suchanek, 1985; Nicastro et al., 2020). Thus, accumulation of plastics within mussel beds could have knock-on effects on the numerous organisms depending on these aggregations. Indeed, there is increasing literature indicating that habitat-forming species represent an efficient pathway for MPs from water to marine benthic herbivores (e.g., Gutow et al., 2016; Zhao et al., 2018; Saley et al., 2019). Additionally, the vertical gradient in MPs within the mussel bed (shells vs. base) is likely to have different effects on the infauna inhabiting distinct layers of the mussel bed; this effect is likely to be greater in multi-layered mussel beds.

5. Conclusion

Plastic pollution is projected to increase in the future as estimates predict > 6 Mt. of solid waste will be produced daily by the global urban population by 2025 (Hoornweg et al., 2013; Lebreton and Andrady, 2019). Our results highlight how, in a world where intraspecific variation is a common feature of natural communities and plastic pollution is increasingly becoming a ubiquitous threat across ecosystems, species can show undetected, cryptic variation among populations. This level of diversity could, in turn, shape the response of the species as a whole to plastic pollution.

In the case of mussel beds as biogenic habitats, endolith-induced shell erosion is also predicted to increase as a result of ongoing ocean acidification and warming rates (Tribollet et al., 2009; Reyes-Nivia et al., 2013). Thus, the presence of symbiotic endolithic microbes may increasingly shape MP trapping and retention by intertidal mussel beds, particularly at low wave-exposure sites, where the modulating effect of infestation is greater, and at low latitudes, where levels of infestation are more pronounced. Because these microbes are found not only in intertidal mussel species but also in other biogenic habitats such as coral reefs, our results suggest that the observed increased risk of MP contamination and pollution may not be limited to mussel beds.

CRediT authorship contribution statement

K.R.N. and G.I.Z. conceived the idea; all authors contributed to the experimental design; G.I.Z. conducted the field sampling; G.I.Z., K.R.N. and L.S. conducted the laboratory work; L.S. and K.R.N. analysed the data; K.R.N. led the writing of the manuscript with contributions from all authors.

Declaration of competing interest

The authors declare that they have no known competing financial interests or personal relationships that could have appeared to influence the work reported in this paper.

Acknowledgments

This research was funded by Fundação para a Ciência e a Tecnologia (FCT - MEC, Portugal (grant number: UIDB/04326/2020, EXPL/BIA-BMA/0682/2021), the National Research Foundation of South Africa (grant number: 64801), a Pierre Hubert Curien PESSOA grant, both the European Maritime and Fisheries Fund (FEAMP) and France Filière Pêche through the research project SOLACE. This work is a contribution to the CPER research project CLIMIBIO. The authors thank the French Ministère de l'Enseignement Superieur et de la Recherche, the Hauts de France Region and the European Funds for Regional Economical Development for their financial support to this project.

Appendix A. Supplementary data

Supplementary data to this article can be found online at https://doi.org/10.1016/j.scitotenv.2022.153922.

References

Anderson, M.J., 2006. Distance-based tests for homogeneity of multivariate dispersions. Biometrics. 62, 245–253.
Arya, S., 1975. A drag partition theory for determining the large-scale roughness parameter and wind stress on the Arctic pack ice. J. Geophys. Res. 80, 3447–3454.
Bergstrom, D.J., Kotey, N.A., Tachie, M.F., 2002. The effects of surface roughness on the mean velocity profile in a turbulent boundary layer. J. Fluids Eng. 124, 664–670.
Burchard, H., Baumert, H., 1998. The formation of estuarine turbidity maxima due to density effects in the salt wedge. A hydrodynamic process study. J. Phys. Oceanogr. 28, 309–321.
Butman, C.A., Fréchette, M., Geyer, W.R., Starczak, V.R., 1994. Flume experiments on food supply to the blue mussel *Mytilus edulis* L. as a function of boundary-layerflow. Limnol. Oceanogr. 39, 1755–1768.
Chriss, T., Caldwell, D.R., 1982. Evidence for the influence of form drag on bottom boundary layer flow. J.Geophys.Res.Oceans 87, 4148–4154.
Clarke, K.R., Gorley, R.N., 2006. PRIMER v6: User Manual/Tutorial. PRIMER-E, Plymouth UK.
Clarke, K.R., Somerfield, P.J., Chapman, M.G., 2006. On resemblance measures for ecological studies, including taxonomic dissimilarities and a zero-adjusted Bray–Curtis coefficient for denuded assemblages. J. Exp. Mar. Biol. Ecol. 1, 55–80.
Commito, J.A., Rusignuolo, B.R., 2000. Structural complexity in mussel beds: the fractal geometry of surface topography. J. Exp. Mar. Biol. Ecol. 255, 133–152.
Cozzolino, L., Nicastro, K.R., Zardi, G.I., de los Santos, C.B., 2020. Species-specific plastic accumulation in the sediment and canopy of coastal vegetated habitats. Sci. Total Environ. 723, 138018.
D'Onghia, G., Calculli, C., Capezzuto, F., Carlucci, R., Carluccio, A., Grehan, A., Indennidate, A., Maiorano, P., Mastrototaro, F., Pollice, A., 2017. Anthropogenic impact in the Santa Maria di Leuca cold-water coral province (Mediterranean Sea): observations and conservation straits. Deep-Sea Res. II Top. Stud. Oceanogr. 145, 87–101.
Dehaut, A., Cassone, A.L., Frère, L., Hermabessiere, L., Himber, C., Rinnert, E., Rivière, G., Lambert, C., Soudant, P., Huvet, A., Duflos, G., Paul-Pont, I., 2016. Microplastics in seafood: benchmark protocol for their extraction and characterization. Environ. Pollut. 215, 223–233.
Denny, M., 1995. Predicting physical disturbance: mechanistic approaches to the study of survivorship on wave-swept shores. Ecol. Monogr. 65, 371–418.
Denny, M.W., Gaylord, B., 2010. Marine ecomechanics. Annu. Rev. Mar. Sci. 2, 89–114.
Denny, M.W., Shibata, M., 1989. Consequences of surf-zone turbulence for settlement and external fertilization. Am. Nat. 134, 859–889.
Des Roches, S., Post, D.M., Turley, N.E., Bailey, J.K., Hendry, A.P., Kinnison, M.T., Schweitzer, J.A., Palkovacs, E.P., 2018. The ecological importance of intraspecific variation. Nat.Ecol. Evol. 2, 57–64.
Drobnitch, S.T., Nickols, K., Edwards, M., 2017. Abiotic influences on bicarbonate use in the giant kelp, Macrocystis pyrifera in the Monterey Bay. J. Phycol. 53, 85–94.
Evans, G.T., 1989. The encounter speed of moving predator and prey. J. Plankton Res. 11, 415–417.
Farrell, P., Nelson, K., 2013. Trophic level transfer of microplastic: Mytilus edulis (L.) to Carcinus maenas (L.). Environ. Pollut. 177, 1–3.
Feldhaar, H., 2011. Bacterial symbionts as mediators of ecologically important traits of insect hosts. Ecol. Entom. 36, 533–543.
Fuchs, H.L., Reidenbach, M.A., 2013. Biophysical constraints on optimal patch lengths for settlement of a reef-building bivalve. PLoS One 8, e71506.
Gillson, L., Dawson, T.P., Jack, S., McGeoch, M.A., 2013. Accommodating climate change contingencies in conservation strategy. Trends Ecol. Evol. 28, 135–142.
Green, M.O., Hewitt, J.E., Thrush, S.F., 1998. Seabed drag coefficient over natural beds of horse mussels (Atrina zelandica). J. Mar. Res. 56, 613–637.
Green, D.S., Boots, B., O'Connor, N.E., Thompson, R., 2016. Microplastics affect the ecological functioning of an important biogenic habitat. Environ.Sci.Technol 51, 68–77.
Green, D.S., Colgan, T.J., Thompson, R.C., Carolan, J.C., 2019. Exposure to microplastics reduces attachment strength and alters the haemolymph proteome of blue mussels (Mytilus edulis). Environ. Pollut. 246, 423–434.
Gündoğdu, S., Çevik, C., 2017. Micro-and mesoplastics in Northeast Levantine coast of Turkey: the preliminary results from surface samples. Mar. Pollut. Bull. 118, 341–347.
Gutow, L., Eckerlebe, A., Giménez, L., Saborowski, R., 2016. Experimental evaluation of seaweeds as a vector for microplastics into marine food webs. Environ.Sci.Technol. 50, 915–923.
Hidalgo-Ruz, V., Gutow, L., Thompson, R.C., Thiel, M., 2012. Microplastics in the marine environment: a review of the methods used for identification and quantification. Environ. Sci.Technol. 46, 3060–3075.
Hoornweg, D., Bhada-Tata, P., Kennedy, C., 2013. Environment: waste production must peak this century. Nature News. 502, p. 615.
Huang, W., Chen, M., Song, B., Deng, J., Shen, M., Chen, Q., Zeng, G., Liang, J., 2020. Microplastics in the coral reefs and their potential impacts on corals: a mini-review. Sci. Total Environ., 143112
Hurtado, P., Prieto, M., Aragón, G., de Bello, F., Martínez, I., 2020. Intraspecific variability drives functional changes in lichen epiphytic communities across Europe. Ecology 101, e03017.
Jones, C.G., Lawton, J.H., Shachak, M., 1994. Organisms as ecosystem engineers. Oikos 69, 373–386.
Kaehler, S., 1999. Incidence and distribution of phototrophic shell-degrading endoliths of the brown mussel Perna perna. Mar. Biol. 135, 505–514.
Kaehler, S., McQuaid, C.D., 1999. Lethal and sub-lethal effects of phototrophic endoliths attacking the shell of the intertidal mussel Perna perna. Mar. Biol. 135, 497–503.
Kaplan-Hallam, M., Bennett, N.J., Satterfield, T., 2017. Catching sea cucumber fever in coastal communities: conceptualizing the impacts of shocks versus trends on social-ecological systems. Glob. Environ. Chang. 45, 89–98.

Katrak, G., Dittmann, S., Seuront, L., 2008. Spatial variation in burrow morphology of the mud shore crab Helograpsus haswellianus (Brachyura, Grapsidae) in South Australian saltmarshes. Mar. Freshw. Res. 59, 902–911.
Khan, M.B., Prezant, R.S., 2018. Microplastic abundances in a mussel bed and ingestion by the ribbed marsh mussel Geukensia demissa. Mar. Pollut. Bull. 130, 67–75.
Krause-Jensen, D., Lavery, P., Serrano, O., Marbà, N., Masque, P., Duarte, C.M., 2018. Sequestration of macroalgal carbon: the elephant in the Blue Carbon room. Biol. Lett. 14, 20180236.
Krogstadt, P.Å., Antonia, R.A., 1999. Surface roughness effects in turbulent boundary layers. Exp. Fluids 27, 450–460.
Lacoste, É., Weise, A.M., Lavoie, M.-F., Archambault, P., McKindsey, C.W., 2019. Changes in infaunal assemblage structure influence nutrient fluxes in sediment enriched by mussel biodeposition. Sci. Total Environ. 692, 39–48.
Lapointe, L., Bourget, E., 1999. Influence of substratum heterogeneity scales and complexity on a temperate epibenthic marine community. Mar. Ecol. Prog. Ser. 189, 159–170.
Law, K.L., 2017. Plastics in the marine environment. Annu. Rev. Mar. Sci. 9, 205–229.
Lebreton, L., Andrady, A., 2019. Future scenarios of global plastic waste generation and disposal. Palgrave Commun. 5, 6.
Lim, H.S., Fraser, A., Knights, A.M., 2020. Spatial arrangement of biogenic reefs alters boundary layer characteristics to increase risk of microplastic bioaccumulation. Environ. Res. Lett. 15, 064024.
Loh, T.-L., Archer, S.K., Dunham, A., 2019. Monitoring program design for data-limited marine biogenic habitats: a structured approach. Ecol.Evol. 9, 7346–7359.
Lourenço, C.R., Zardi, G.I., McQuaid, C.D., Serrão, E.A., Pearson, G.A., Jacinto, R., Nicastro, K.R., 2016. Upwelling areas as climate change refugia for the distribution and genetic diversity of a marine macroalga. J. Biogeogr. 43, 1595–1607.
Lourenço, C.R., Nicastro, K.R., McQuaid, C.D., Chefaoui, R.M., Assis, J., Taleb, M.Z., Zardi, G.I., 2017a. Evidence for rangewide panmixia despite multiple barriers to dispersal in a marine mussel. Sci. Rep. 7, 10279.
Lourenço, C.R., Nicastro, K.R., McQuaid, C.D., Sabour, B., Zardi, G.I., 2017b. Latitudinal incidence of phototrophic shell-degrading endoliths and their effects on mussel bed microclimates. Mar. Biol. 164, 129.
Mann, K., Lazier, J., 1991. Dynamics of Marine Ecosystem. Blakwell Sci., Michigan, United States of America, pp. 23–90.
Mathalon, A., Hill, P., 2014. Microplastic fibers in the intertidal ecosystem surrounding Halifax Harbor, Nova Scotia. Mar. Pollut. Bull. 81, 69–79.
Mato, Y., Isobe, T., Takada, H., Kanehiro, H., Ohtake, C., Kaminuma, T., 2001. Plastic resin pellets as a transport medium for toxic chemicals in the marine environment. Environ. Sci.Technol. 35, 318–324.
Menge, B.A., 1976. Organization of the New England Rocky Intertidal Community: role of predation, competition, and environmental heterogeneity. Ecol. Monogr. 46, 355–393.
MERI, 2015. Guide to Microplastic Identification. Marine & Environmental Research Institute (MERI), New York City.
Meriam, J.L., Kraige, L.G., Bolton, J.N., 2020. Engineering Mechanics: Dynamics. John Wiley & Sons.
Monin, A.S., Yaglom, A.M., 2013. Statistical fluid mechanics. Mechanics of Turbulence. vol. II. Courier Corporation.
Mota, C.F., Engelen, A.H., Serrão, E.A., Pearson, G.A., 2015. Some don't like it hot: microhabitat-dependent thermal and water stresses in a trailing edge population. Funct. Ecol. 29, 640–649.
Ndhlovu, A., McQuaid, C.D., Nicastro, K., Marquet, N., Gektidis, M., Monaco, C.J., Zardi, G., 2019. Biogeographical patterns of endolithic infestation in an invasive and an indigenous intertidal marine ecosystem engineer. Diversity 11, 75.
Ndhlovu, A., McQuaid, C.D., Nicastro, K.R., Zardi, G.I., 2021. Community succession in phototrophic shell-degrading endoliths attacking intertidal mussels. J. Molluscan Stud. 87 (1), eyaa036.
Ndhlovu, A., McQuaid, C.D., Monaco, C.J., 2021. Ectoparasites reduce scope for growth in a rocky-shore mussel (Perna perna) by raising maintenance costs. Sci. Total Environ. 753, 142020.
Nel, H.A., Froneman, P.W., 2018. Presence of microplastics in the tube structure of the reef-building polychaete Gunnarea gaimardi (Quatrefages 1848). Afr. J. Mar. Sci. 40, 87–89.
Nicastro, K.R., Zardi, G.I., McQuaid, C.D., 2008. Movement behaviour and mortality in invasive and indigenous mussels: resilience and resistance strategies at different spatial scales. Mar. Ecol. Prog. Ser. 372, 119–126.
Nicastro, K.R., Zardi, G.I., Teixeira, S., Neiva, J., Serrao, E.A., Pearson, G.A., 2013. Shift happens: trailing edge contraction associated with recent warming trends threatens a distinct genetic lineage in the marine macroalga Fucus vesiculosus. BMC Biol. 11, 6.
Nicastro, K.R., McQuaid, C.D., Zardi, G.I., 2018. Between a rock and a hard place: combined effect of trampling and phototrophic shell-degrading endoliths in marine intertidal mussels. Mar. Biodivers. 1–6.
Nicastro, K.R., McQuaid, C.D., Dievart, A., Zardi, G.I., 2020. Intraspecific diversity in an ecological engineer functionally trumps interspecific diversity in shaping community structure. Sci. Total Environ. 743, 140723.
Nikora, V., Goring, D., Biggs, B., 1997. On stream periphyton-turbulence interactions. N. Z. J. Mar. Freshw. Res. 31, 435–448.
Nikora, V., Green, M.O., Thrush, S.F., Hume, T.M., Goring, D., 2002. Structure of the internal boundary layer over a patch of pinnid bivalves (Atrina zelandica) in an estuary. J. Mar. Res. 60, 121–150.
Ntuli, N.N., Nicastro, K.R., Zardi, G.I., Assis, J., McQuaid, C.D., Teske, P.R., 2020. Rejection of the genetic implications of the "Abundant Centre Hypothesis" in marine mussels. Sci. Rep. 10, 604.
Paine, R.T., Levin, S.A., 1981. Intertidal landscapes: disturbance and the dynamics of pattern. Ecol. Monogr. 51, 145–178.
Perkins-Kirkpatrick, S.E., Lewis, S.C., 2020. Increasing trends in regional heatwaves. Nat. Commun. 11, 3357.
Piarulli, S., Airoldi, L., 2020. Mussels facilitate the sinking of microplastics to bottom sediments and their subsequent uptake by detritus-feeders. Environ. Pollut. 266, 115151.
Reyes-Nivia, C., Diaz-Pulido, G., Kline, D., Guldberg, O.H., Dove, S., 2013. Ocean acidification and warming scenarios increase microbioerosion of coral skeletons. Glob. Chang. Biol. 19, 1919–1929.
Rutherford, J.C., 1994. River Mixing. John Wiley, Hoboken, N. J.
Saada, G., Nicastro, K.R., Jacinto, R., McQuaid, C.D., Serrao, E.A., Pearson, G.A., Zardi, G.I., 2016. Taking the heat: distinct vulnerability to thermal stress of central and threatened peripheral lineages of a marine macroalga. Divers. Distrib. 22, 1060–1068.
Saley, A.M., Smart, A.C., Bezerra, M.F., Burnham, T.L.U., Capece, L.R., Lima, L.F.O., Carsh, A.C., Williams, S.L., Morgan, S.G., 2019. Microplastic accumulation and biomagnification in a coastal marine reserve situated in a sparsely populated area. Mar. Pollut. Bull. 146, 54–59.
Schneider, C.A., Rasband, W.S., Eliceiri, K.E., 2012. NIH Image to ImageJ: 25 years of image analysis. Nat. Methods 9, 671–675.
Seuront, L., 2010. Fractals And Multifractals in Ecology And Aquatic Science. CRC Press.
Seuront, L., Schmitt, F.G., 2005a. Multiscaling statistical procedures for the exploration of biophysical couplings in intermittent turbulence. Deep-Sea Res.II 52, 1308–1324.
Seuront, L., Schmitt, F.G., 2005b. Multiscaling statistical procedures for the exploration of biophysical couplings in intermittent turbulence. Part II. Applications. Deep-Sea Res. II Top. Stud. Oceanogr. 52, 1325–1343.
Seuront, L., Schmitt, F., Lagadeuc, Y., 2001. Turbulence intermittency, small-scale phytoplankton patchiness and encounter rates in plankton: where do we go from here? Deep-Sea Res. I Oceanogr. Res. Pap. 48, 1199–1215.
Seuront, L., Yamazaki, H., Schmitt, F., 2004. Intermittency. In: Baumert, H., Sündermann, J., Simpson, J. (Eds.), Marine Turbulences: Theories, Observations And Models. Cambridge University Press, Cambridge.
Seuront, L., Nicastro, K.R., Zardi, G.I., Goberville, E., 2019. Decreased thermal tolerance under recurrent heat stress conditions explains summer mass mortality of the blue mussel Mytilus edulis. Sci. Rep. 9, 17498.
Seuront, L., Nicastro, K.R., McQuaid, C.D., Zardi, G.I., 2021. Microplastic leachates induce species-specific trait strengthening in intertidal mussels. Ecol. Appl. 31 (1), e02222.
Smale, D.A., Wernberg, T., Oliver, E.C.J., Thomsen, M., Harvey, B.P., Straub, S.C., Burrows, M.T., Alexander, L.V., Benthuysen, J.A., Donat, M.G., Feng, M., Hobday, A.J., Holbrook, N.J., Perkins-Kirkpatrick, S.E., Scannell, H.A., Sen Gupta, A., Payne, B.L., Moore, P.J., 2019. Marine heatwaves threaten global biodiversity and the provision of ecosystem services. Nat. Clim. Chang. 9, 306–312.
Sousa, W.P., 1984. Intertidal mosaics: patch size, propagule availability, and spatially variable patterns of succession. Ecology 1918–1935.
Suchanek, T., 1985. Mussels and their role in structuring rocky shore communities. The Ecology of Rocky Coastes, pp. 70–96.
Sugihara, G., May, R.M., 1990. Applications of fractals in ecology. Trends Ecol. Evol. 5, 79–86.
Teuten, E.L., Saquing, J.M., Knappe, D.R.U., Barlaz, M.A., Jonsson, S., Björn, A., Rowland, S.J., Thompson, R.C., Galloway, T.S., Yamashita, R., Ochi, D., Watanuki, Y., Moore, C., Viet, P.H., Tana, T.S., Prudente, M., Boonyatumanond, R., Zakaria, M.P., Akkhavong, K., Ogata, Y., Hirai, H., Iwasa, S., Mizukawa, K., Hagino, Y., Imamura, A., Saha, M., Takada, H., 2009. Transport and release of chemicals from plastics to the environment and to wildlife. Philos.Trans.R.Soc.B: Biol.Sci. 364, 2027–2045.
Tribollet, A., Godinot, C., Atkinson, M., Langdon, C., 2009. Effects of elevated pCO2 on dissolution of coral carbonates by microbial euendoliths. Glob. Biogeochem. Cycles 23.
Van Duren, L.A., Herman, P.M., Sandee, A.J., Heip, C.H., 2006. Effects of mussel filtering activity on boundary layer structure. J. Sea Res. 55, 3–14.
Widdows, J., Brinsley, M.D., Salkeld, P.N., Elliott, M., 1998. Use of annular flumes to determine the influence of current velocity and bivalves on material flux at the sediment-water interface. Estuaries 21, 552–559.
Wright, L., Friedrichs, C., Hepworth, D., 1997. Effects of benthic biology on bottom boundary layer processes, Dry Tortugas Bank, Florida Keys. Geo-Mar. Lett. 17, 291–298.
Zar, J., 1999. Biological Statistics. Prentice Hall, Upper Saddle River, NJ.
Zardi, G.I., Nicastro, K.R., McQuaid, C.D., Rius, M., Porri, F., 2006. Hydrodynamic stress and habitat partitioning between indigenous (Perna perna) and invasive (Mytilus galloprovincialis) mussels: constraints of an evolutionary strategy. Mar. Biol. 150, 79–88.
Zardi, G.I., Nicastro, K.R., McQuaid, C.D., Gektidis, M., 2009. Effects of endolithic parasitism on invasive and indigenous mussels in a variable physical environment. PLoS One 4, e6560.
Zardi, G., Nicastro, K., McQuaid, C., Ng, T., Lathlean, J., Seuront, L., 2016. Enemies with benefits: parasitic endoliths protect mussels against heat stress. Sci. Rep. 6, 31413.
Zardi, G.I., Monsinjon, J.R., McQuaid, C.D., Seuront, L., Orostica, M., Want, A., Firth, L.B., Nicastro, K.R., 2021. Foul-weather friends: modelling thermal stress mitigation by symbiotic endolithic microbes in a changing environment. Glob. Chang. Biol. 27 (11), 2549–2560.
Zhao, S., Ward, J.E., Danley, M., Mincer, T.J., 2018. Field-based evidence for microplastic in marine aggregates and mussels: implications for trophic transfer. Environ.Sci.Technol. 52, 11038–11048.